SUPPORTING INFORMATION

Photoelectrochemical Behavior of PEDOT/Nanocarbon Electrodes: Fundamentals and Structure–Property Relationships

Attila Kormányos[a,b], Dorottya Hursán[a,b], Csaba Janáky[a,b,*]

[a] MTA-SZTE „Lendület" Photoelectrochemistry Research Group, Rerrich Square 1, Szeged, H-6720, Hungary

[b] Department of Physical Chemistry and Materials Science, University of Szeged, Rerrich Square 1, Szeged, H-6720, Hungary

*E-mail: janaky@chem.u-szeged.hu

Table of contents

1. Stability of PEDOT under irradiation (GC-BID data)

CPs are generally unstable under UV-light irradiation. Long-term photoelectrolysis measurements, performed in Ar-saturated 0.1 M Na_2SO_4 using UV-irradiation, proved that this problem also holds for PEDOT (see Figure S1 for the gas-chromatography data). When PEDOT was illuminated by UV-light, carbon monoxide and methane was detected in the gas phase. The appearance of these products in the absence of any external carbon source can only correspond to the degradation of PEDOT. Contrastingly, when a solar simulator was used as a light source (and the UV component, i.e., λ < 400 nm was filtered), there was no CO or CH_4 formation.

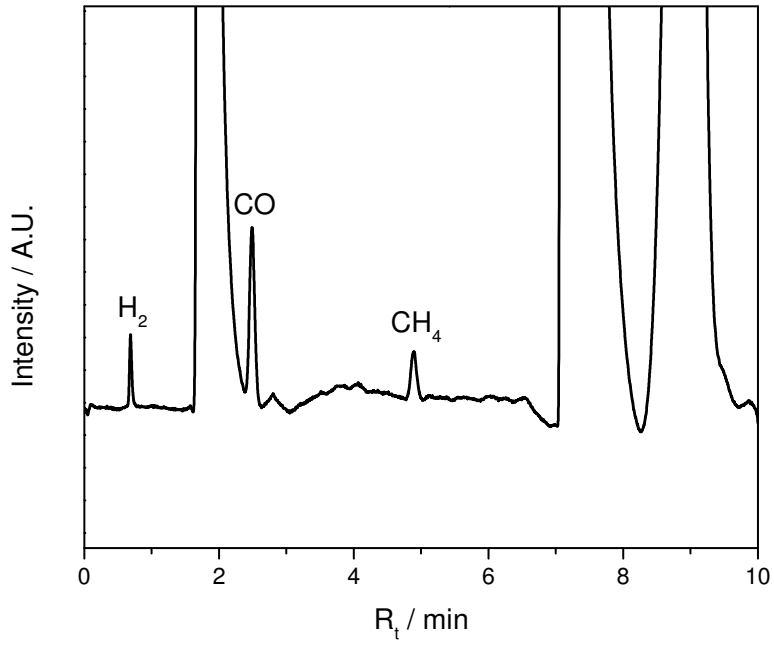

Figure S1. Gas-chromatogram, recorded during the long-term photoelectrolysis experiment, performed on a PEDOT photoelectrode, applying UV irradiation (300 W Hg–Xe UV lamp) in Ar-saturated 0.1 M Na_2SO_4.

2. Preparation of the photoelectrodes

First, both CNT and graphene were spray-coated on a glassy carbon (GC) substrate. The mass of the spray-coated nanocarbons was determined by using an analytical microbalance. Then, the electrochemical surface area of each nanocarbon-coated electrode was measured prior to the polymerization procedure. After registering the cyclic voltammograms for the various nanocarbon films, the charge capacitance values were calculated and normalized with the value, derived for a 1 cm^2, smooth GC electrode. The results are presented in Figure S2 by plotting the normalized charge capacitance versus the spray-coated mass.

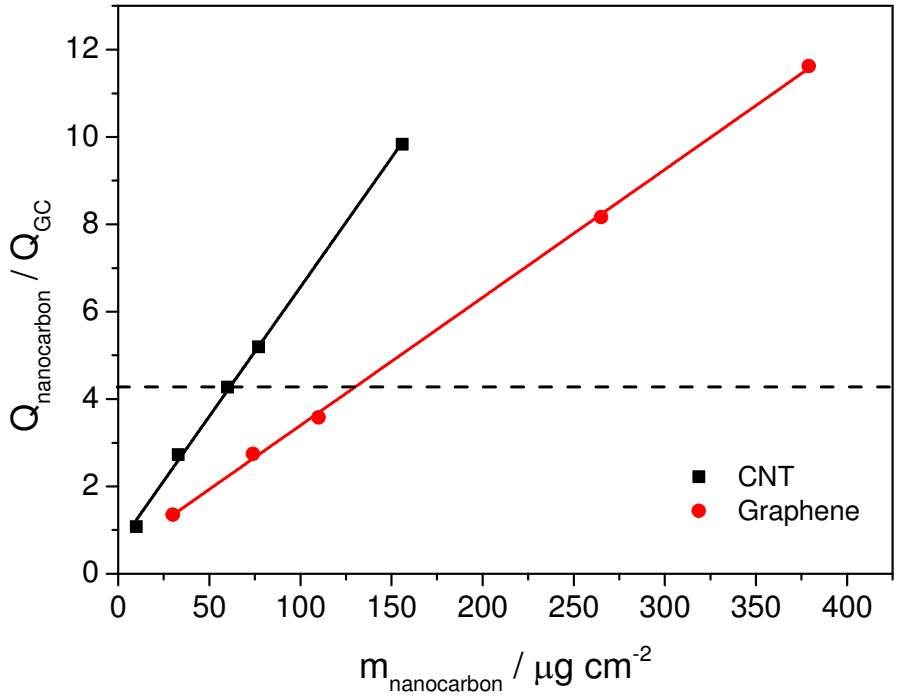

Figure S2. Normalized charge capacitance vs. spray-coated mass curves calculated for each graphene/GC (black squares) and CNT/GC layer (blue dots). The dashed line indicates the mass, which was used during measurements when the electrochemically active surface of the nanocarbons were identical.

By applying this representation, it can be concluded that the measured charge capacitance increases linearly with the increasing mass. Additionally, the charge capacitance values are higher in the case of the GC/CNT layers.

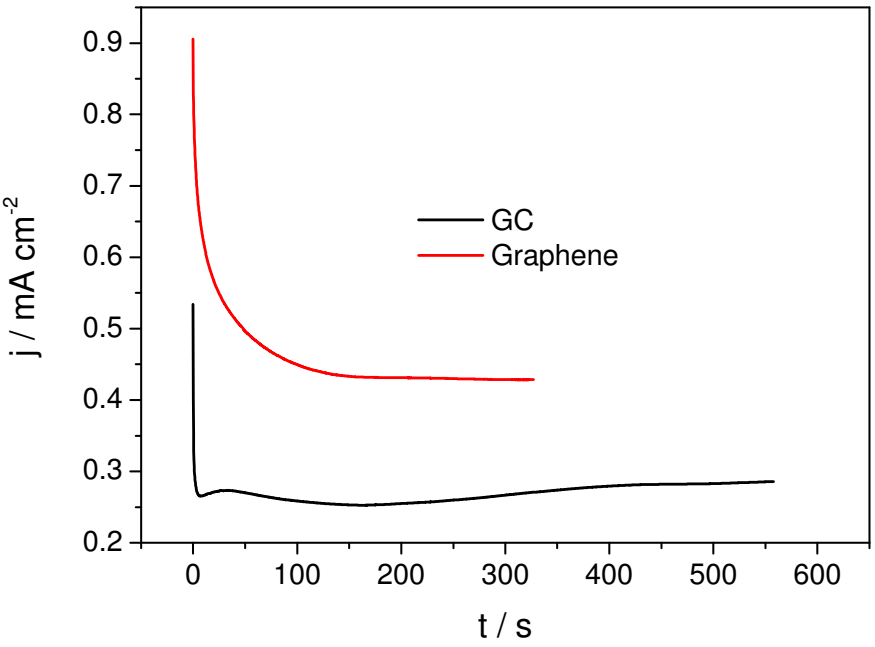

Figure S3. Chronoamperometric polymerization curves, recorded during the electrodeposition of PEDOT on the surface of a bare GC (black curve), and a graphene-coated GC (red curve) electrode ($m_{graphene}$ = 110 µg cm^{-2}, Q_{cutoff} = 150 mC cm^{-2}).

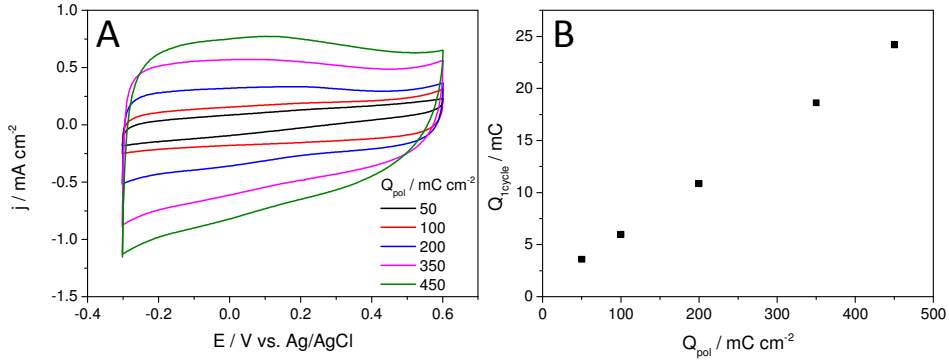

Figure S4. (A) Comparison of cyclic voltammograms recorded for PEDOT/graphene nanocomposite electrodes ($m_{graphene}$ = 110 µg cm^{-2}) synthesized with different PEDOT loading in 0.1 M Na_2SO_4 solution, saturated with Ar (υ = 50 mV s^{-1}) (B) Calculated charge passed during the cycle vs. polymerization charge density plot for various PEDOT/graphene electrodes.

3. SEM and HR-TEM images

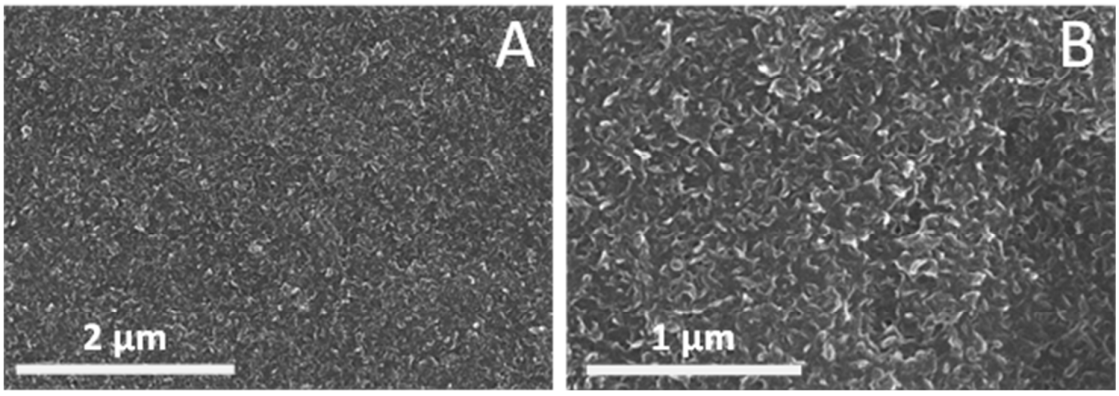

Figure S5. SEM images of a bare PEDOT layer on GC (Q_{cutoff} = 50 mC cm^{-2}), collected at 25000× (A) and at 50000× (B) magnification.

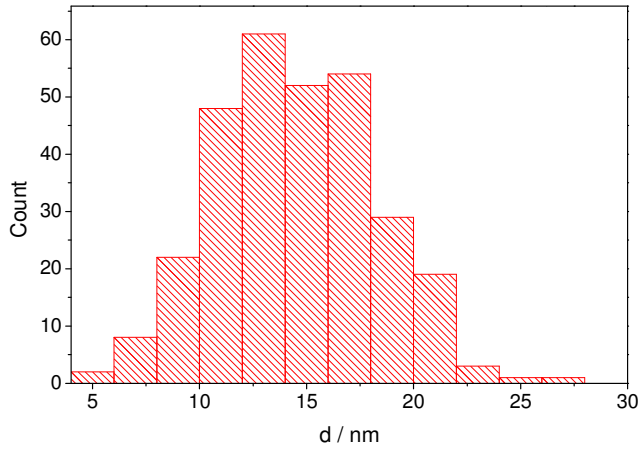

Figure S6. Histogram, corresponding to the diameter-dependence of the bare CNTs, calculated from the SEM images that are presented in Figure 4A.

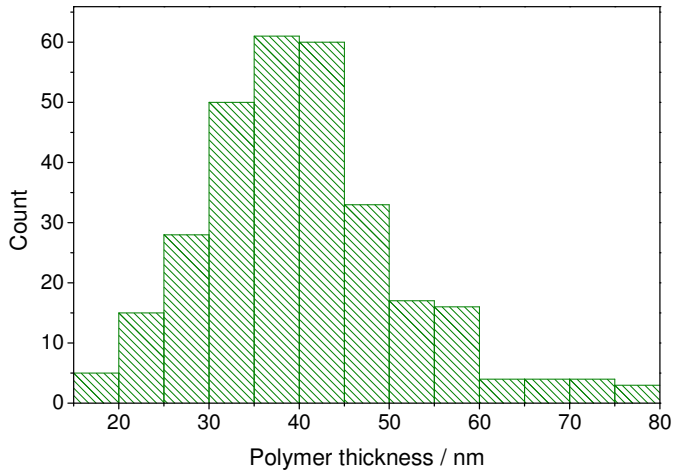

Figure S7. PEDOT thickness dependence calculated from Figure 4A, B, and C, using Equation 1

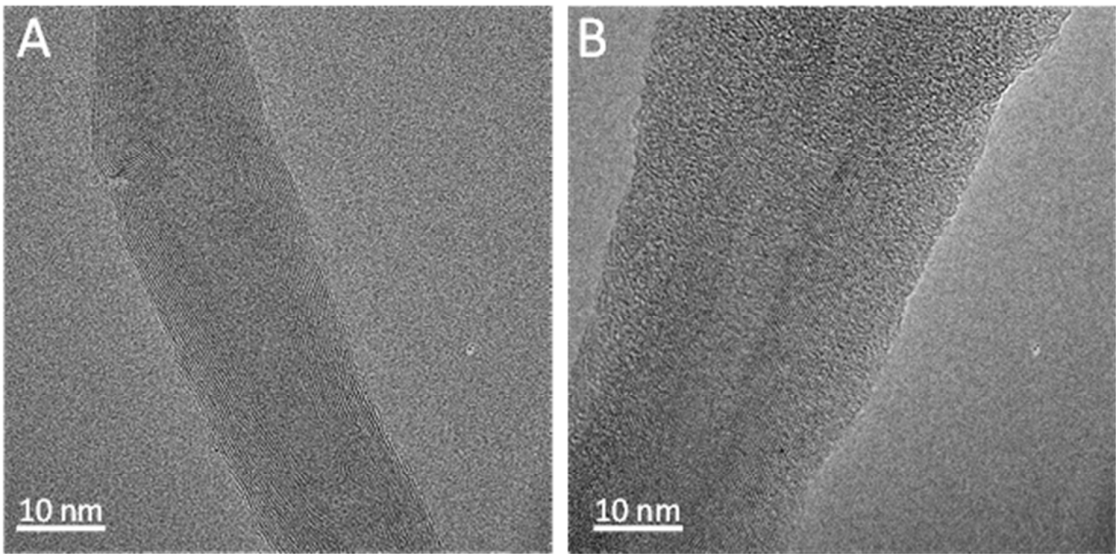

Figure S8. HR - TEM images captured for a (A) bare CNT, and (B) PEDOT/CNT nanocomposite layer. The magnification was 620000× in both cases.

4. Assignation of the characteristic Raman bands of PEDOT

Table S1. Assignation of the characteristic Raman bands of PEDOT

Raman Shift / cm^{-1}	Assignment[1–4]
578 991	Oxyethylene ring deformation
699	Symmetric C–S–C deformation
1090 1124	C–O–C deformation
1270	C_{α}–$C_{\alpha'}$ (inter-ring) stretching
1368	C_{β}–C_{β} stretching
1434	symmetric C_{α}=C_{β}(–O) stretching

5. Photovoltammetry data

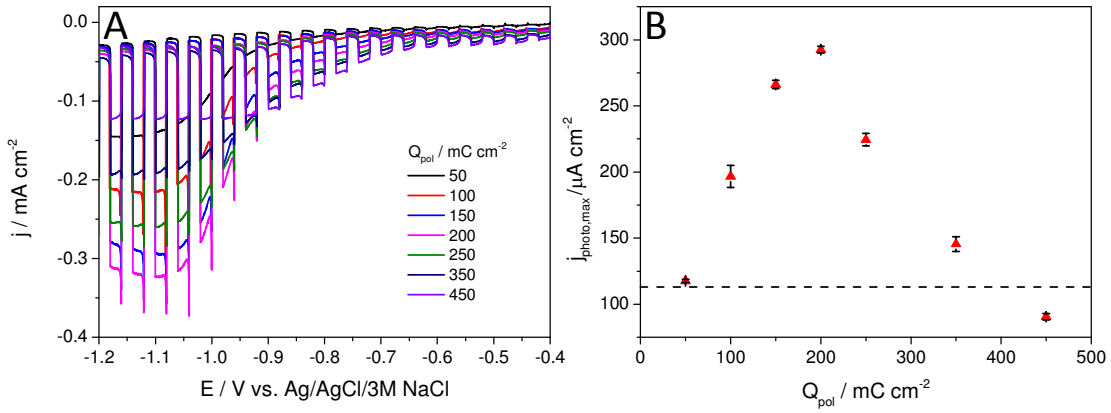

Figure S9. (A) Comparison of the photovoltammograms, recorded in Ar - saturated 0.1 M Na_2SO_4 for the nanocomposites prepared with different PEDOT/graphene ratio by varying the polymerization charge density ($m_{graphene}$ = 110 µg cm^{-2}). (B) Maximum photocurrent vs. polymerization charge density plot, calculated from the data presented in Figure S9A. The dashed line marks the highest photocurrent, harvested for the best-performing PEDOT photoelectrode.

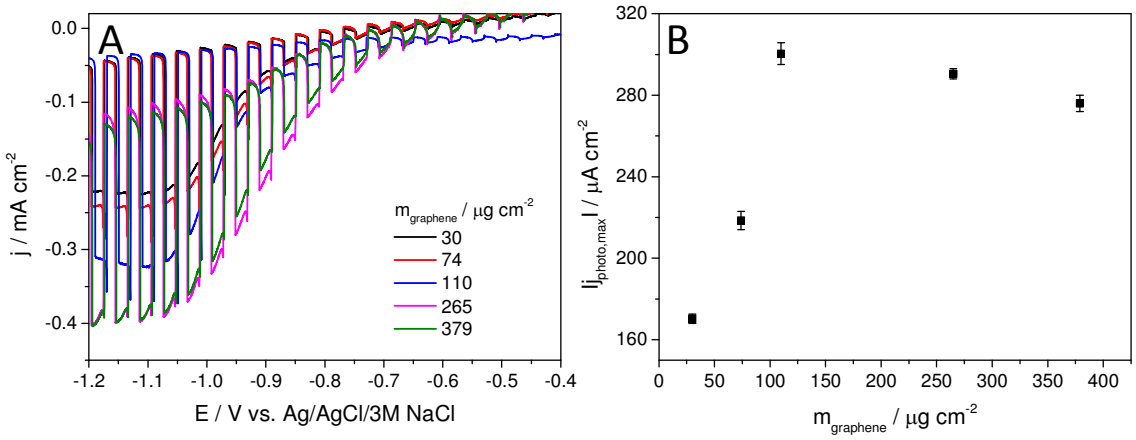

Figure S10. (A) Comparison of photovoltammograms, recorded in Ar-saturated 0.1 M Na_2SO_4 for the nanocomposites prepared with the same PEDOT/graphene ratio, but varying the graphene loading. (B) Maximum photocurrent vs. spray coated graphene mass plot, calculated from the data presented in Figure S10A. Measurements were carried out applying 2 mV s^{-1} sweep rate, 0.1 Hz chopping frequency, and a solar simulator (200 mW cm^{-2}) as a light source.

6. CPD and APS measurements

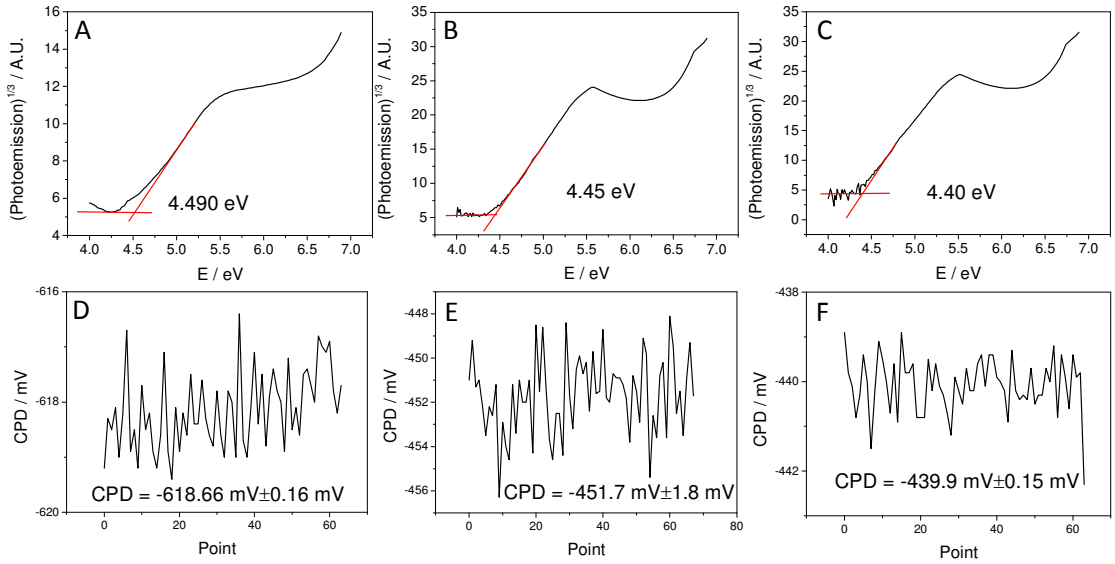

Figure S11. APS measurements, recorded for (A) PEDOT (Q_{cutoff} = 50 mC cm^{-2}), a (B) PEDOT/CNT (m_{CNT} = 60 µg cm^{-2}, Q_{cutoff} = 400 mC cm^{-2}), and (C) for a PEDOT/graphene layer ($m_{graphene}$ = 110 µg cm^{-2}, Q_{cutoff} = 200 mC cm^{-2}). CPD measurements recorded for (D) PEDOT (Q_{cutoff} = 50 mC cm^{-2}), a (E) PEDOT/CNT (m_{CNT} = 60 µg cm^{-2}, Q_{cutoff} = 400 mC cm^{-2}), and (F) for a PEDOT/graphene layer ($m_{graphene}$ = 110 µg cm^{-2}, Q_{cutoff} = 200 mC cm^{-2}).

7. EIS data

To study the effect of different nanocarbons on the electrical properties of the nanocomposites, EIS measurements were carried out. Electrochemical impedance spectra of the PEDOT and PEDOT/nanocarbon layers were recorded in a 1 M Na_2SO_4 solution saturated with Ar, at −0.9 V potential, in the 10 Hz to 10 kHz frequency range, using a sinusoidal excitation signal (10 mV RMS amplitude). Modulus weighted fitting was performed using the Nova Software of the Autolab Instrument.

Figure S12A shows the Nyquist plots recorded for the bare PEDOT and CNT layers, and for the PEDOT/CNT nanocomposites prepared with different PEDOT loadings. Data, recorded for PEDOT/graphene is shown in Figure S13. In the case of PEDOT, a distinct semicircle was identified in the high-frequency range, corresponding to the charge-transfer limited process, whereas the linear part, observed in the lower-frequency range can be assigned to the diffusion-limited electron-transfer process.[5,6] In the case of the CNT and graphene, a straight line with an almost 90° inclination and with a very small semicircle portion was observed. This is characteristic to the capacitive behavior of both nanocarbons.[6]

There are two important trends upon composite formation: the diameter of the semicircle portion in the high-frequency range shrunk compared to the bare PEDOT, along with the inclination of the linear section of the curves, in the low-frequency range. These phenomena have been already discussed in the literature for both PEDOT /nanocarbon[7–9] and for other conducting polymer/nanocarbon electrodes.[10,11] By electrodepositing PEDOT on any type of conducting nanocarbon network, the electric conductivity of the nanocomposite layers improved. This results in better charge carrier transport therefore suppressed charge carrier recombination, which might explain the higher observed photocurrents in the case of the PEDOT/CNT and PEDOT/graphene layers in our study. The increasing thickness of PEDOT in both nanocomposites lead to semicircles with slightly larger diameters. However, the diameter of these semicircles in the high-frequency portion of the spectra were less than ≈ 10 Ω, even when the highest amount of PEDOT is present on the CNT surface. These observations were also confirmed by the Bode plots where the shape of the curves was almost identical for all three PEDOT/CNT nanohybrids (Figure S12B and Figure S13B for the PEDOT/graphene system).

These qualitative observations were quantified by fitting an equivalent circuit to the experimental data. The fitted equivalent circuit is discussed in detail in the Supporting Information (Figure S14), along with some examples, regarding the precision of the fit (Figure S15). The calculated charge transfer resistance (R_{ct}) was 406 Ω for the pristine PEDOT, which value is higher than the ones, reported in the literature earlier. This difference can be explained by the fact that our EIS measurements were carried out at a potential (E = −0.9 V), where PEDOT was in its fully reduced state, instead of the open circuit conditions or potentials, where PEDOT is slightly or fully oxidized. The R_{ct} values were very small for the CNT and graphene (2 Ω and 5 Ω) films, verifying that these nanocarbons have high electrical conductivity. Electrodepositing PEDOT on the surface of the nanocarbon scaffolds only slightly changed the charge transfer properties (i.e., R_{ct} was less than 10 Ω in all cases). In conclusion, by electrodepositing PEDOT on the surface of both CNTs and graphene, the conductivity of these composites can be highly improved, which might result in better charge carrier transport (i.e., higher harvestable photocurrents).

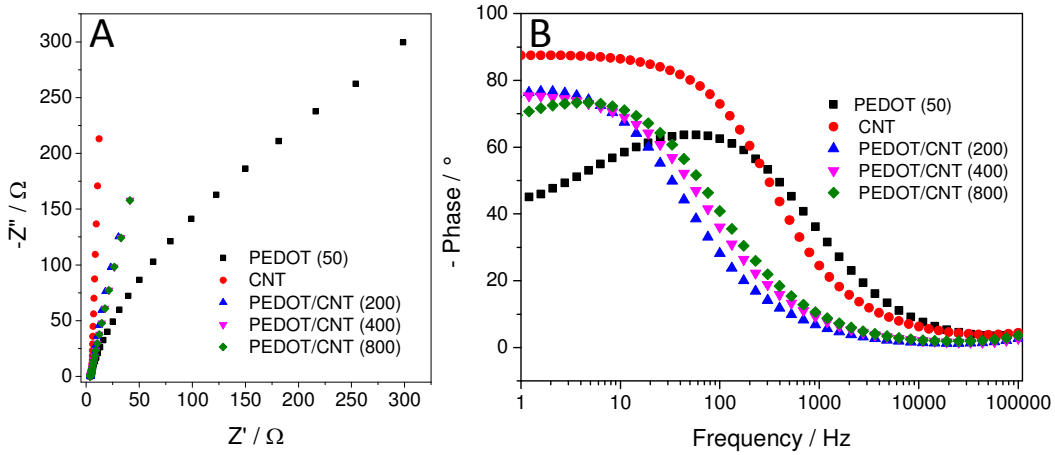

Figure S12. (A) Nyquist plots recorded for PEDOT and PEDOT/CNT composites with varying PEDOT content, and (B) Bode plots recorded for PEDOT and PEDOT/CNT composites with varying PEDOT content. Data were recorded in 1 M Na_2SO_4 solution saturated with Ar at E = -0.9 V potential, in the 0.1 Hz - 100 kHz frequency range. The values in the brackets are indicating the polymerization charge density used to deposit the PEDOT layers.

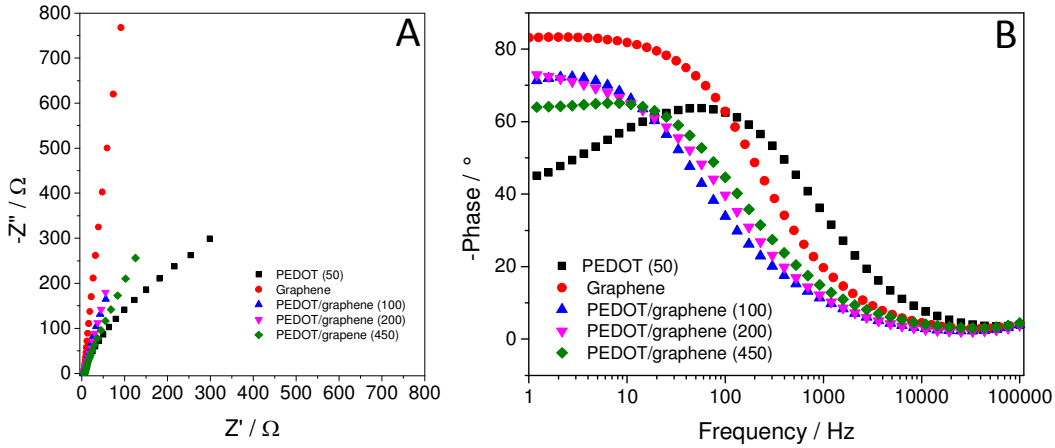

Figure S13. Nyquist plots recorded for PEDOT and PEDOT/graphene composites with varying PEDOT content (A) and Bode plots recorded for PEDOT and PEDOT/graphene composites with varying PEDOT content (B), in 1 M Na_2SO_4 solution saturated with Ar at E = -0.9 V potential, in the 0.1 Hz - 100 kHz frequency range. The values in the brackets are indicating the polymerization charge density used to deposit the PEDOT layers.

A modified Randles circuit was used to fit the experimental EIS data (Figures 9 and S12). The circuit consists the following elements: an equivalent solution resistance (R_s), a charge transfer resistance (R_{ct}), a Warburg diffusion element, attributable to SO_4^{2-} anions moving in and out of the PEDOT layer, a Faradaic pseudocapacitance (C_F) assigned to the polymer film, and a double-layer capacitance (C_{dl}).[11–14]

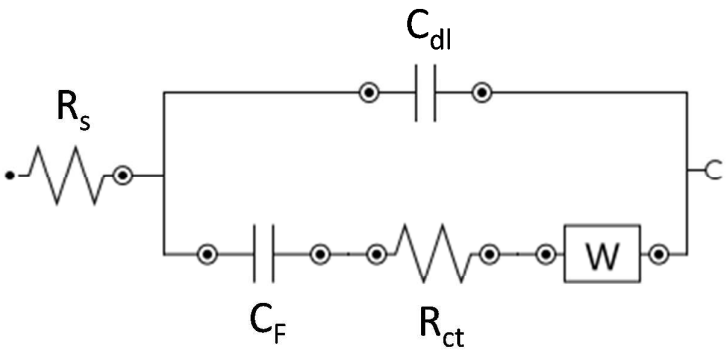

Figure S14. Equivalent circuit fitted on the measured EIS data presented in Figures 9 and S14.

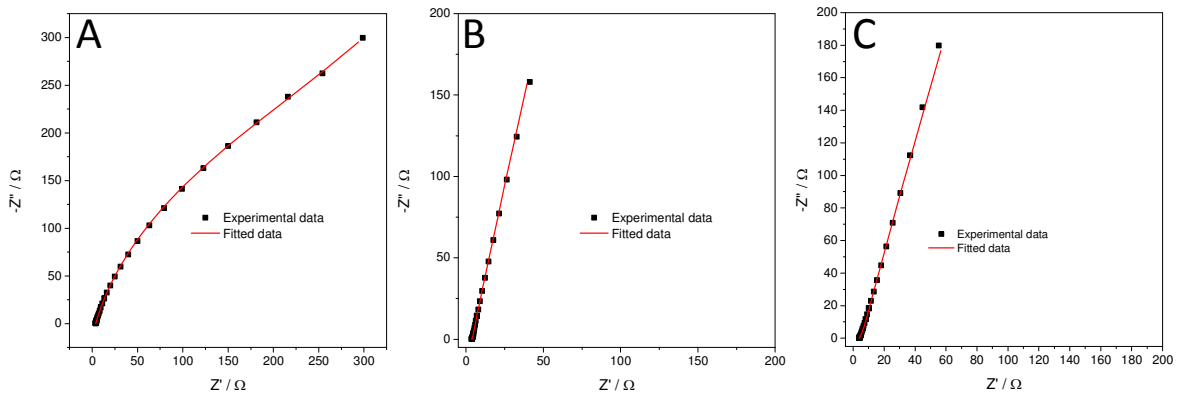

Figure S15. Accuracy of the fit, using the equivalent circuit presented in Fig. S9, demonstrated on the data, recorded for a (A) PEDOT (Q_{cutoff} = 50 mC cm^{-2}), a (B) PEDOT/CNT (m_{CNT} = 60 µg cm^{-2}, Q_{cutoff} = 400 mC cm^{-2}), and (C) for a PEDOT/graphene layer ($m_{graphene}$ = 110 µg cm^{-2}, Q_{cutoff} = 200 mC cm^{-2}) in 1 M Na_2SO_4 solution saturated with Ar, at −0.9 V potential, from the 0.1 Hz to 100 kHz frequency range.

8. References

(1) Zhou, C.; Liu, Z.; Du, X.; Ringer, S. P. Electrodeposited PEDOT Films on ITO with a Flower-like Hierarchical Structure. *Synth. Met.* **2010**, *160*, 1636–1641.

(2) Sakmeche, N.; Aaron, J. J.; Fall, M.; Aeiyach, S.; Jouini, M.; Lacroix, J. C.; Lacaze, P. C. Anionic Micelles; a New Aqueous Medium for Electropolymerization of poly(3,4-Ethylenedioxythiophene) Films on Pt Electrodes. *Chem. Commun.* **1996**, 2723-2724.

(3) Jin, L.; Wang, T.; Feng, Z.-Q.; Leach, M. K.; Wu, J.; Mo, S.; Jiang, Q. A Facile Approach for the Fabrication of Core–shell PEDOT Nanofiber Mats with Superior Mechanical Properties and Biocompatibility. *J. Mater. Chem. B* **2013**, *1*, 1818-1825.

(4) Garreau, S.; Louarn, G.; Buisson, J. In Situ Spectroelectrochemical Raman Studies of Poly (3, 4-ethylenedioxythiophene)(PEDT). *Macromolecules* **1999**, *32*, 6807-6812.

(5) Sen, P.; De, A. Electrochemical Performances of poly(3,4-ethylenedioxythiophene)–$NiFe_2O_4$ Nanocomposite as Electrode for Supercapacitor. *Electrochim. Acta* **2010**, *55*, 4677–4684.

(6) Aboutalebi, S. H.; Chidembo, A. T.; Salari, M.; Konstantinov, K.; Wexler, D.; Liu, H. K.; Dou, S. X. Comparison of GO, GO/MWCNTs Composite and MWCNTs as Potential Electrode Materials for Supercapacitors. *Energy Environ. Sci.* **2011**, *4*, 1855-1865.

(7) Yang, Q.; Pang, S.-K.; Yung, K.-C. Study of PEDOT–PSS in Carbon Nanotube/conducting Polymer Composites as Supercapacitor Electrodes in Aqueous Solution. *J. Electroanal. Chem.* **2014**, *728*, 140–147.

(8) Braik, M.; Barsan, M. M.; Dridi, C.; Ben Ali, M.; Brett, C. M. A. Highly Sensitive Amperometric Enzyme Biosensor for Detection of Superoxide Based on Conducting polymer/CNT Modified Electrodes and Superoxide Dismutase. *Sensors Actuators, B Chem.* **2016**, *236*, 574–582.

(9) Nabilah Azman, N. H.; Lim, H. N.; Sulaiman, Y. Effect of Electropolymerization Potential on the Preparation of PEDOT/graphene Oxide Hybrid Material for Supercapacitor Application. *Electrochim. Acta* **2016**, *188*, 785–792.

(10) Wu, G.; Li, L.; Li, J.-H.; Xu, B.-Q. Polyaniline-Carbon Composite Films as Supports of Pt and PtRu Particles for Methanol Electrooxidation. *Carbon N. Y.* **2005**, *43*, 2579–2587.

(11) Ramya, R.; Sivasubramanian, R.; Sangaranarayanan, M. V. Conducting Polymers-Based Electrochemical supercapacitors—Progress and Prospects. *Electrochim. Acta* **2013**, *101*, 109–129.

(12) Sahoo, S.; Karthikeyan, G.; Nayak, G. C.; Das, C. K. Electrochemical Characterization of in Situ Polypyrrole Coated Graphene Nanocomposites. *Synth. Met.* **2011**, *161*, 1713–1719.

(13) Zhang, J.; Kong, L.-B.; Wang, B.; Luo, Y.-C.; Kang, L. In-Situ Electrochemical Polymerization of Multi-Walled Carbon Nanotube/polyaniline Composite Films for Electrochemical Supercapacitors. *Synth. Met.* **2009**, *159*, 260–266.

(14) Zou, W.; Wang, W.; He, B.; Sun, M.; Wang, M.; Liu, L.; Xu, X. Effects of Counterions on Pseudocapacitance Performance of Polyaniline in Sulfuric Acid and P-Toluene Sulphonic Acid Electrolyte. *J. Electroanal. Chem.* **2010**, *641*, 111–118.